PCCP

Accepted Manuscript

ROYAL SOCIETY OF CHEMISTRY

www.rsc.org/pccp

Role of Tryptophans in UV-B Absorption of UVR8 Photoreceptor– A Computational Study

Qi Wu[1], Bolong Huang[1], T.A. Niehaus[2], Xiaojing Yang[3], Jun Fan[1*] and Rui-Qin Zhang[1*]

[1]*Departmentof Physics and Materials Science, City University of Hong Kong, Hong Kong SAR, China*

[2]*Institute I - Theoretical Physics, University of Regensburg, D-93040 Regensburg, Germany*

[3]*Department of Chemistry, University of Illinois at Chicago, Chicago, IL 60607, USA*

Abstract

Arabidopsis thaliana UV RESISTANCE LOCUS8 (UVR8) has been identified as a photoreceptor for ultraviolet-B (UV-B). Tryptophan (Trp) residues have been shown to play a critical role in the response to UV-B irradiation in UVR8. In this work, we explore the spectroscopic behaviors of Trps in different protein environments of the UVR8 structure using the time-dependent density functional tight-binding (TD-DFTB) scheme. We show that W233 exhibits the longest absorption wavelength, highlighting its potential as a terminal Trp chromophore in UV-B harvesting antenna. Our electronic and optical property analyses using various amino acid models support the important roles of W285 and W233 in sensing UV-B light at longer absorption wavelengths (~290 nm). We also provide evidence for the specific function ofW94 in absorption at the longest wavelengths (305.8 nm in cluster II and 304.5 nm in cluster III). To these findings, we also add information about the influence of the arginine and aspartic acid residues surrounding the Trp pyramid on the particular absorption bands (280~300 nm) that are characteristic of the UV-B photoreceptor.

Keywords: UV RESISTANCE LOCUS 8 (UVR8), tryptophan chromophore, UV-B response, spectroscopic behavior,

Introduction

Ultraviolet-B radiation (UV-B; 280-315 nm) is a minor component of sunlight but has a strong impact on living organisms. In plants, UV-B perception is necessary for UV-B acclimation, affecting their growth and development as an environmental stimulus. Specific UV-B perception is mediated by the photoreceptor UV RESISTANCE LOCUS 8 (UVR8) recently identified in *Arabidopsis thaliana.*[1-3] UVR8 exists as a homodimer in plant cells but rapidly dissociates into monomers following exposure to UV-B.[4] In contrast to all other known photoreceptors, UVR8 lacks the external cofactor photochrome. Instead, it perceives UV-B signals using built-in tryptophans (Trps). [4-7]

Crystal structures[6, 7] show that *At*UVR8 contains 13 UV-absorbing Trp residues (see Fig. 1b).[7] Six (W39, W92, W144, W196, W300 and W352) are evenly distributed along six blades, distant from the dimer interface (Fig. 1c); and seven (W94, W198, W233, W250, W285, W302 and W337) are buried at the homodimeric interface (Fig. 1d).[6, 8] The proposed excitonically coupled Trp pyramid responsible for UV-B sensing is formed by W94 atop and the Trp triad W233, W285 and W337. Absorption of UV-B by one or more 'pyramid' Trps, with a primary role established for W233 and W285,[9, 10] leads to disruption of salt bridges involving critical arginine and aspartic acids; followed by dimer destabilization and dissociation.[7] This basic understanding is further corroborated by quantum chemical calculations which show an effective charge-transfer state involving W233 and W285, suggesting W233 as a sink for the excitation energy transferred from other Trp within the protein.[11]

Despite these insights, the exact link between Trp residues and UV-B absorption within the UVR8 protein environment remains unclear. To date no experimental or computational data have been published which show the individual UV-B absorption behavior of each Trp residue and the excitonically coupled Trp pyramid. Although Wu *et al*.[12] report the absorption spectra of UVR8 amino acid clusters, the local protein environment, including the neighboring ariginine and aspartic acid residues, and the solvent water molecules, were not included in their exploration of the optical properties of Trp. More importantly, there is no direct evidence for the significant role of individual W233 and W285 and the contributions of each Trp pyramid member to UV-B absorption. Therefore, theoretical simulations are required to elucidate the functionality of Trps in UV-B perception at the atomic level, particularly the spectrophysics of the excitonically coupled

Trp pyramid and the extended pyramid clusters with local residues included in UVR8.

In this paper, we use the density functional tight-binding (DFTB),[13, 14] and its time-dependent linear response extension TD-DFTB[15, 16] scheme to address the problem of computing the absorption properties of individual Trp chromophores and also their excitonically coupled amino acid clusters within the environment of UVR8. It is well established that the optical properties of Trps in protein are determined by both the conformation and the microenvironment. To address the effect of conformation, we investigate the saturation of the truncated atoms in respect of the substituent effects on the absorption spectra of individual Trp residue. With regard to the microenvironment of UVR8, we explore the absorption sequence to analyze the diverse absorption behavior of each Trp with local residues included. We also present an interpretation of the absorption peaks of Trp pyramid within UVR8. TD-DFTB is computationally efficient and opens up the possibility of including large parts of the neighboring protein environment. We develop several amino acid models that aid our understanding of UV-B photoreception of UVR8, by calculating the Trp spectra and identifying the effects of substitution, local neighboring residues, and the extended environment on various electronic transitions.

Computational Details

In this work, the Trp molecules and their adjacent residues were cut from the X-ray crystal structure[7] of the UVR8 protein (Protein Data Bank ID: 4DNW) and no optimization was performed in order to ensure a spatial distribution equivalent to the experimental conditions. The TD-DFTB scheme was chosen to study the electronic and optical properties of various Trp. As an approximation to time-dependent density functional theory (TD-DFT), the TD-DFTB method following the TD-DFT route of Casida[17,18] is capable of efficiently handling the excited-state calculations of very large systems. Details of the method and benchmarks against more sophisticated quantum chemical methods can be found elsewhere. [15, 16]

To validate the reliability of the present approach, calculations were firstly performed for indole rings for which experimental information is available. We compare the calculated absorption energies for the two low-lying π->π* valence singlet excited states named L_b and L_a with that from a CASSCF/CASPT2 study as well as the experimental data (see Table 1). For instance, the L_b state computed at 4.39 eV (f = 0.059) agrees well with the results obtained using the CASSCF/CASPT2 method and the reported experimental data. Both TD-DFTB and

CASSCF/CASPT2 underestimated the oscillator strength for the L_a state. However the absorption energy is shown to be 4.64eV, close to the experimental value of 4.77eV, proving that the TD-DFTB method is reliable in dealing with Trp residues.

To further testify the reliability of TD-DFTB in treating larger indole extended systems, we also calculate the absorption energies for the low-lying singlet excited states L_b and L_a for a stacking dimer of Trp W285 and W337. The calculated absorption energies are compared with the results of TD-DFT at the B3LYP/6-31+G(d,p) level[12,19] (see Table S1). TD-DFT was chosen instead of CASSCF/CASPT2, since it is more computationally efficient in treating the tryptophan dimer. Compared with the TD-DFT results, the difference in the transition energies is around 0.15 eV. The B3LYP functional is known to blue-shift excitations by 0.1-0.2 eV for non charge-transfer (CT) excitations, and the double for absorptions involving CT, relative to experiments.[20, 21] Therefore the difference in transition energies between TD-DFTB and the experimental data is also acceptable. In general, these comparisons confirm that TD-DFTB offers acceptable accuracy to investigate the absorption properties of the large indole extended systems, and enables our study to be extended from several atoms to very large amino acid clusters with the neighboring protein environment included.

Based on the TD-DFTB theory, we study the absorption properties of individual Trp chromophores as well as their excitionically coupled amino acid clusters with respect to the backbone truncation and the microenvironment within the UVR8. For individual Trps, we investigate the effect of different substituents and the local residues on their absorption spectra in order to investigate the diverse absorption behavior of each Trp. Additionally, the spectrophysics of these excitonically coupled Trps in the complete Trp pyramid is explored to reveal the effects of local and extended environments on the various electronic transitions.Moreover, we provide an interpretation of the absorption peaks of several amino acid cluster models that aid our understanding of UV-B photoreception of UVR8.

Results and discussion

The findings obtained for various substituted Trp residues and various clustering of Trp from the pyramid in UVR8 are presented in three sections. The absorption properties of individual Trp residue are discussed with respect to the backbone truncation and the microenvironment within the UVR8 structure. To this end, we firstly investigate Trp in the gas phase, using various substituents

at the carboxyl and amino termini in order to find suitable truncated models for an amino acid in a peptide chain. In the second step, the individual Trp molecule is simulated by considering its geometries in an experimental X-ray structure. In this way the influence of the conformational factors on the absorption spectra can be studied. Additionally, we explore at this stage the order of absorption energies when local neighboring residues such as interfacial waters are included in the simulation. Finally, the spectrophysics of these excitonically coupled Trps in the complete Trp pyramid is explored in relation to the effects of local and extended environments on the various electronic transitions.

Substituent Effect on the Absorption Spectra of Individual Trp Residue

In this work, the six Trp residues (W39, W92, W144, W196, W300 and W352) distant from the dimer interface are denoted as "distal Trp". The other seven (W94, W198, W233, W250, W302, W285 and W337) at the dimer interface are denoted as "interfacial Trp". The chemical structure of a Trp residue is depicted in Fig. 2. R and R' stand for the substitutes attached to the truncated atoms (the C or N termini) and are marked with asterisks. The Trp residues were truncated so that in principle only the functional group, extended by one N or C atom, was retained in the model. R and R' can be hydrogen, hydroxyl or methyl group. In addition, the peptide bonds formed between Trp and the neighboring amino acid residues (that is, the formyl group), are also considered at the R and R' sites. We therefore developed a total of nine models using different substitutes at sites R and R', where M1 is treated as the reference system. To avoid confusion with the original O atom linked to the C terminus, the O atoms added at the R and R' sites are marked with O' and O^* respectively. We analyzed the substituent effects by investigating the spectral shifts upon substitution with respect to the absorption peak of M1. Interfacial Trps display diverse orientations in the indole ring orientations in relation to the backbone chain atoms. Only the absorption spectra of W94, W285, W233 and W337 are illustrated in Fig. 3. The absorption spectra of other interfacial Trp in other substitution models can be found in Fig. S1.

As shown in Fig. 3, a predominant feature of the calculated absorption spectra of all Trps studied is a strong band from 280 nm to 315nm. Experimentally, the first absorption wavelength for Trp is usually found at 280 nm.[23] Previous theoretical calculations of the first peak at the optimization level B3LYP/6-31+G(d,p) is predicted to be at 270nm.[12] Using the *w*B97XD functional with the same basis set gives an additional blue-shift, of ~15 nm.[12] In contrast, our

current TD-DFTB calculations predict the first absorption peak at 280 nm, which is in good agreement with the experimental data. In general, M2, M4, M5, M7 and M8 feature a pronounced red-shift compared to the absorption peaks of M1, while the other models (M3, M6 and M9) induce obvious blue-shifts in the absorption peaks of interfacial Trp.

The transition molecular orbital plots of W233 (Fig. 4), are used to characterize the substituent effects on the distribution of the molecular orbitals of Trp. For M1, the electron transition is from the π orbital of the indole ring to the π^* orbital of the indole ring and the n_p orbital of the O atom. In M2, the substitution of a methyl group at the R' site introduces electron transfer from the n_p orbital of the N and O atoms to the π^* orbital of the indole ring. The observed red-shift in M4 is due to the unshared *p*-electrons of the substitution of the hydroxyl at the R site. Consequently, the substitutions in M5 also induce a red-shift in the absorption peak in contrast to that of M1. M7 also shows a red-shift due to the substitution of the methyl group at the N terminus. It donates electrons from the n_p orbital located on the O and N atoms to the π^* orbital of the indole rings. The absorption peaks of M5 and M8 therefore also induce a red-shift in the absorption peak in contrast to that of M1. Additionally, M3, M6 and M9 show an obvious blue-shift in the absorption peak in relation to that of M1, due to the effect of the formyl substitute at the R' site. Taken together, these results provide evidence that the substitution at the R and R' sites would strongly influences the absorption properties of Trp residues. The substitution of hydroxyl and methyl groups at the R site causes a red-shift in the absorption spectra of Trp, whereas the substitution of formyl group at R' site induces a blue-shift (no larger than 5 nm) in the absorption spectra of Trp. The neighboring residues and functional group of Trp itself therefore should be considered carefully in simulating the spectrophysics of amino acids within the protein.

The Order of Absorption Peaks for Individual Trp Residues in UVR8

The above discussion of substituent effects allows us to further compare the characteristic absorption peaks of the 13 Trps within UVR8. We specifically examine the order of the absorption peaks of each Trp. In the practical calculations, the effect of neighboring residues is also considered when calculating these absorption properties. For each interfacial Trp W198, W250, W302 and W337, adjacent water molecules (see Fig. 5a-5d) form hydrogen bonds with the indole nitrogens of Trps and may influence their absorption properties. Therefore, interfacial waters are also included in our calculations of the absorption spectra. For W94 and W233, the N atom of the

indole ring forms a hydrogen bond with the carboxyl group of the adjacent D96 and D129, respectively (Fig. 5e and 5f). We therefore include the neighboring carboxyl group when we investigate the resultant absorption spectrum. In the case of W285, there is no key water molecule or neighboring carboxyl group. We hence calculate for the isolate W285 molecule without including neighboring residues. To examine the diverse absorption behavior and function of Trp in UV-B perception, we plot the absorption spectra for each truncated model. Fig. 6 shows M7 as an example of the absorption spectra. This includes a peptide bond particularly susceptible to UV radiation and reflects the main chain geometry of a protein structure. The absorption spectra of other truncation models plots can be found in Fig. S2.

As shown in Fig. 6, the TD-DFTB calculations reveal that the interfacial Trp exhibit overlapping absorption bands that cover almost the entire UV-B range (280-315 nm); In contrast, the absorption maxima of the other amino acids contained in UVR8 are no longer than 280 nm (Fig. S3), suggesting the dominant role of Trps as a UV-B chromophore in UVR8. Distal Trp exhibits similar absorption peaks due to having a largely identical backbone and rotameric conformations. The insolated Trp W94, W250 and W285 have the longest absorption wavelength (Fig. 6). If the microenvironment is considered, D129 introduces a ~20 nm red-shift in the absorption of W233, which is consistent with simulation results using ONIOM (SAC-CI:AMBER) theory.[24] W233 accordingly has the longest absorption. Similarly, the inclusion of the carboxyl group of D96 induces a 15nm red-shift in the absorption peak of W94, which ranks second in the absorption sequence next to W233. W198, W337 and W302 have the first, second, and third shortest wavelength absorptions, while W250 and W285 in the middle of the order of absorption peaks. We propose that the interfacial Trp residues may constitute a light-harvesting antenna by capturing UV-B photons and thus act as actuators to generate a biological signal via dimer dissociation.[25] It is well known that it is difficult to determine the pathway of the excitons transferred among interfacial Trp just by the absorption order of each Trp. However, given that W233 has the longest absorption wavelength of the nine models, W233 may serve as the terminal Trp residue in the proposed UV-B harvesting antenna. Our findings are also in good agreement with those of Voityuk *et al*,[11] who show that the protein matrix makes W233 energetically favorable for accepting excitons flowing from other Trp in UVR8. Clearly, further systematic studies are needed to establish the energy transfer pathway of the excitons among interfacial Trp.

Influence of Neighboring Residues on the UV-B Absorption of Clustered UVR8

In this final section, we calculate the absorption spectra of the Trp pyramid with an extended environment, in order to elucidate the functionality and contribution of each of its components after excitonic coupling. Based on the structure of the Trp pyramid, we explore various clusters of amino acid that include Trp, arginine and aspartic acid residues from the UVR8 model. The labeling and numberings of these residues is shown in Fig. 7. Three clusters are investigated to explore the effect of an extended environment on the various electronic transitions of UVR8. Cluster I stands for a bare Trp pyramid (W94/W233/W285/W337). Cluster II includes the additional neighboring residues R286, D96 and D107 (W94/W233/W285/W337/R286/D96/D107). In cluster III, W250 and W302, which are peripheral to the pyramid are also added (W94/W233/W250/W285/W302/W337/R286/D96/D107). An action spectrum of UVR8 shows that although UVR8 has the highest absorption peak around 280 nm the UV-B absorption at ~300 nm is the most physiologically relevant.[9] Hence, only excitation at wavelengths longer than 280 nm and oscillator strengths larger than 0.01 are listed in Table 2, highlighting the effect of the surrounding environment in addition to the chromophore itself.

Cluster I, the Trp pyramid, displays an absorption band within the range 283~296 nm. The longest wavelength of absorption at 295.7 nm corresponds to the electron transfer from orbitals 165 to orbital 172 (see Fig. 9a). The orbital 165 and 172 are mostly occupied on W285. The higher energy absorption at 286.9 nm is mostly from orbital 161 to orbital 170. The electron is transferred from the π orbital of the residue W285 and W233, to the π* orbital of the residue W233. The third absorption peak at 285.8 nm is characterized by electron transfer from orbital 164 to orbital 171 (see Fig. 9), which is strongly localized on W94; the transition is a pure π-π*. The fourth transition at 283.9 nm is mostly from orbital 158 to orbital 169. The electron is transferred from the π orbital of the residue W285 and W337, to the π* orbital of residue W337. These results indicate that W233 and W285 give rise to absorption at the longest wavelength.

When cluster I is extended to cluster II, our TD-DFTB calculations reproduce the shape of the experimental spectrum with a characteristic double peak structure (see Fig. 8). The spectrum displays two absorption bands, at 280-287nm and 290-305nm, which according to our simulations include four main excitations, as listed in Table 2. The longest wavelength absorption (~305.8 nm) is due to the electron transfer from orbital 247 to orbital 264 (Fig. 10). Contributions from the π

orbital of W94 and the σ orbital of D96 are seen in orbital 247, and the π* orbital of W94 is involved in orbital 264. The second shortest wavelength absorption at 299.7 nm originates from electron transfer from orbital 256 to orbital 275, mainly localized on D96. The third absorption at 290.1 nm is related to the electron transfer from orbital 240 to orbital 260. These orbitals are mainly located on the W285 residues with a slight contribution from W233. The fourth absorption at 288.0 nm involves transitions from orbital 253 to orbital 274, mainly occupying on D107. It should be noted that in cluster II the local absorption of W94 occurs at 305.8 nm and of W285 at 290.1 nm. Both values are red-shifted with respect to the isolated Trp residues with absorptions at about 286 nm. The absorption of W285 and W233 occurring at 290.1 nm contributes strongly to the UV-B absorption with a significant oscillator strength of about 0.023.

We further extend the clustered structure to include the neighboring residues W250 and W302 (cluster III). As shown in Fig. 8, cluster III displays a similar spectrum to cluster II, but with enhanced oscillator strength in the 280-287nm range due to the incorporation of residues W250 and W302. The longest wavelength absorption at 304.5 nm is due to electron transfer from orbital 332 to orbital 351 (see Fig. 11). Both of these orbitals are mainly localized on residue W94, but the σ orbital of residues D107 and D96 is involved in orbital 332. Similarly, the second absorption at 291.4 nm displays the largest oscillator strength and an electron transfer from orbital 324 to orbital 346. Again, orbitals 324 and 346 are mainly located on residue W285, with a slight contribution from W233. The third absorption at 291.1 nm involves transitions from orbital 337 to orbital 366, mainly located on D107. The other absorption peaks at 285.6 nm and 280.9 nm correspond to the electron transfer from orbital 309 to orbital 342, and from orbital 321 to orbital 345. Both of these orbitals are localized on residues W302 and W233, respectively.

Based on the above analysis, our calculations show that W285 and W233 dominate the low energy absorption spectrum of the UVR8 Trp pyramid (~290 nm). When more neighboring residues are included, W233 and W285 are responsible for the absorption peaks with the largest oscillator strength, which directly indicates their significant role in initiating the UV-B perception of UVR8. The top of the pyramid, residue W94, contributes significantly to absorption at the longest wavelength due to the effect of neighboring residues (305.8 nm in cluster II and 304.5 nm in cluster III). Our simulations demonstrate that the arginine and aspartic residues surrounding the Trp cluster are also crucial in modulating absorption and strongly influence the absorption spectra

of Trps at longer wavelengths.[24]

Conclusions

In this work, we have investigated the effect of the substitution and local environment on the UV-B absorption of UVR8 due to intrinsic Trps using the TD-DFTB method. The spectral shift upon substitution is discussed with respect to the absorption spectra of ideal Trp without substitution. We show that W233 has the largest absorption wavelength of all Trp residues in UVR8 according to the order of absorption peaks of interfacial Trps. Such a property indicates that W233severs as the terminal UV-B pigment of the UV-B antenna that funnels the UV-B excitation energy. In addition, that is the first work to report the absorption spectrum of the complete Trp pyramid, which shows that W285 and W233 give rise to the absorptions at the longest range (~290 nm) in the Trp pyramid. With more neighboring residues are included, W233 and W285 generate the absorption peaks with the largest oscillator strength, directly demonstrating their significant role as the epicenter of UV-B perception in UVR8. Our results also show the specific function of W94 in the closely packed amino acid clusters for long wavelength absorption (found at 305.8 nm in cluster II and 304.5 nm in cluster III).The arginine and aspartic residues that surround the Trp pyramid also contribute to a shift of the absorption spectra to longer wavelengths. The excitation energies for the various Trp units found in this work may be useful in the parameterization of effective exciton-Hamiltonians, which can shed further light on the detailed exciton dynamics of this system. Our findings of the characteristic absorption behavior of Trp will help further understanding of the UV-B response mechanism of UVR8.

ACKNOWLEDGMENTS

The work described in this paper was supported by a grant from the Research Grants Council of Hong Kong SAR [Project No. CityU103913] and by grants to JF from City University of Hong Kong (Projects No. 7200350 and 9610291).

Table1. Calculated transition energies and oscillator strengths for indole in the gas phase, ΔE means the transition energy, and f stands for the oscillator strength.

	TD-DFTB		CASSCF/CASPT2[26]		Experimental Results [27,28]	
	ΔE (eV)	f	ΔE (eV)	f	ΔE[27](eV)	f[28]
L_b	4.39	0.059	4.43	0.050	4.37	0.045
L_a	4.64	0.040	4.73	0.080	4.77	0.123

Table 2. Lowest excited singlet states (> 280 nm) and their oscillator strengths (f), calculated for the UVR8 clustermodels.

systems[a]	S_1/nm (f)	orbital	S_2/nm (f)	orbital	S_3/nm (f)	orbital	S_4/nm (f)	orbital	S_5/nm (f)	orbital
Cluster I	295.7 (0.013)	165-> 172	286.9 (0.017)	161-> 170	285.8 (0.060)	164-> 171	283.9 (0.032)	158-> 169		
Cluster II	305.8 (0.029)	247-> 264	299.7 (0.015)	256-> 275	290.1 (0.023)	240-> 260	288 (0.047)	253-> 274		
Cluster III	304.5 (0.042)	332-> 351	291.4 (0.025)	324-> 346	291.1 (0.047)	337-> 366	285.6 (0.044)	309-> 342	280.9 (0.034)	321-> 345

[a]Cluster I includes residues W94, W233, W285, and W337. Cluster II includes residues W94, W233, W285, W337, R286, D96 and D107. Cluster III includes residues W94, W233, W250, W285, W302, W337, R286, D96 and D107. These labels are used throughour the paper.

Captions for figures

Fig. 1. Structural model of UVR8 (residues 13-381): (a) side view of the arrangement of tryptophan (W) residues, excluding W400. Tryptophan residues located in the protein core are depicted in blue, whereas those in red reside at the homodimeric interface. (b) as in (a), but viewed from the dimeric interaction surface. (c) top view of the protein core tryptophan residues. (d) top view of the tryptophan residues at the homodimeric interface. Residues that constitute the tryptophan triad are depicted in magenta.

Fig. 2. R-and R'-binding-site geometry of tryptophan represented using a model system. H, C, N and O atoms are colored in white, cyan, blue and red, respectively.

Fig. 3. Absorption spectra[22] of (a) W94, (b) W233, (c) W285 and (d) W337withdifferently substituted models.

Fig. 4. Molecular orbitals involved in the electronic transitions of W233 for differently substituted models.

Fig. 5. Ball and stick models showing the intramolecular hydrogen bond distances (Å)between interfacial tryptophans and the neighboring water molecule or carboxyl group: (a) W198 with water, (b) W250 with water, (c) W302 with water, (d) W337 with water, (e) W94 with carboxyl group of D96 and (f) W233 with carboxyl group of D129.

Fig. 6. Absorption spectra[22]of M7 for distal Trps (top panel), interfacial Trps (middle panel), and interfacial Trps with neighboring residues (bottom panel).

Fig. 7. Configuration of clusters used for calculations of UV absorption spectra of UVR8.

Fig.8. Spectra[22] of the UVR8 amino acid cluster models.

Fig. 9. Active orbitals involved in the transitions for (a) Cluster I at (b) 295.7 nm, (c) 286.9 nm, (d) 285.8 nm and (e) 283.9 nm. Occupied molecular orbitals are plotted on the left panel and unoccupied orbitals are plotted on the right in figures (b) to (e).

Fig. 10. Active orbitals involved in the transitions for (a) Cluster II at (b) 305.8 nm, (c)299.7 nm, (d) 290.1 nm and (e) 288 nm. Occupied molecular orbitals are plotted on the left panel and unoccupied orbitals are plotted on the right in figures (b) to (e).

Fig. 11. Active orbitals involved in the transitions for (a) Cluster III at (b) 304.5 nm, (c) 291.4 nm, (d) 291.1 nm, (e) 285.6 nm and (f) 280.9 nm. Occupied molecular orbitals are plotted on the left

panel and unoccupied orbitals are plotted on the right in figures (b) to (f).

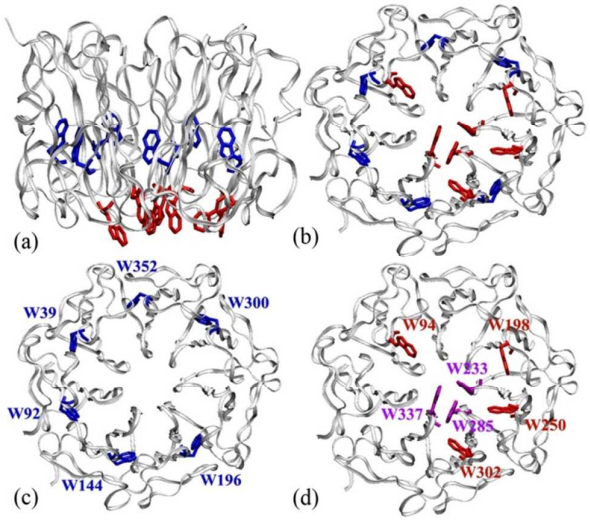

Fig. 1. Structural model of UVR8 (residues 13-381): (a) side view of the arrangement of tryptophan (W) residues, excluding W400. Tryptophan residues located in the protein core are depicted in blue, whereas those in red reside at the homodimeric interface. (b) as in (a), but viewed from the dimeric interaction surface. (c) top view of the protein core tryptophan residues. (d) top view of the tryptophan residues at the homodimeric interface. Residues that constitute the tryptophan triad are depicted in magenta.

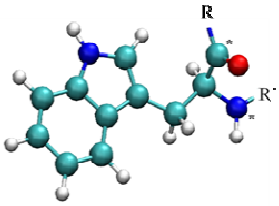

	R	R'
M1	H	H
M2	H	CH3
M3	H	CHO
M4	O'H	H
M5	O'H	CH3
M6	O'H	CHO
M7	N-CH3	H
M8	N-CH3	CH3
M9	N-CH3	CHO

Fig. 2. R-and R'-binding-site geometry of tryptophan represented using a model system. H, C, N and O atoms are colored in white, cyan, blue and red, respectively.

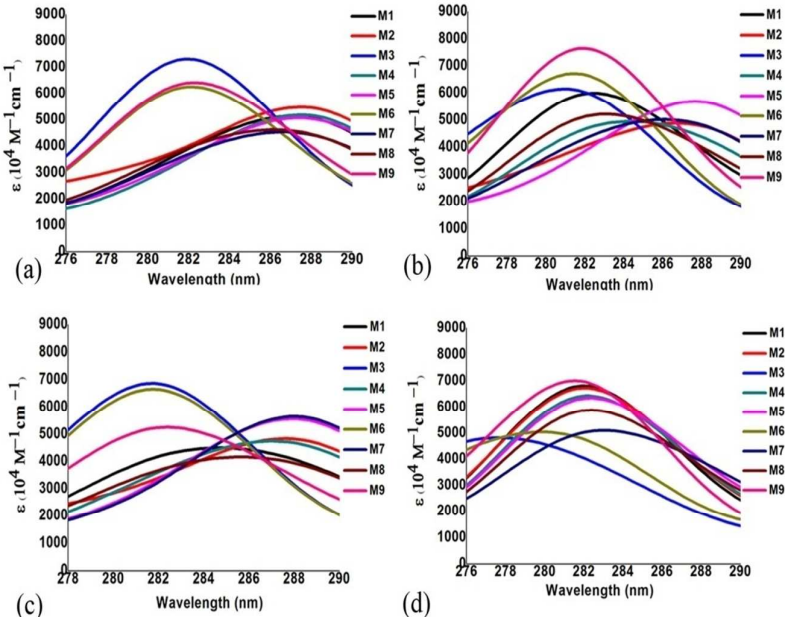

Fig. 3. Absorption spectra[22] of (a) W94, (b) W233, (c) W285 and (d) W337 with differently substituted models.

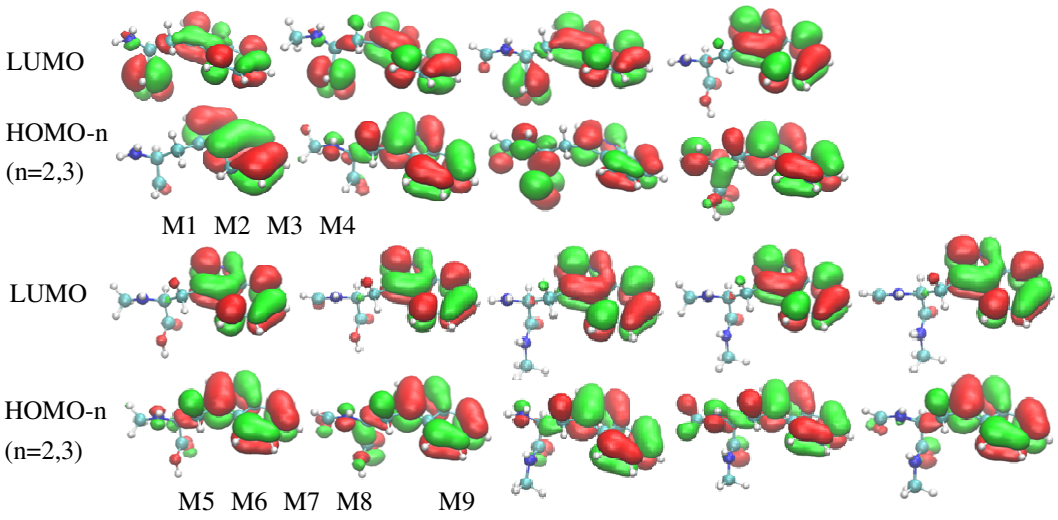

Fig. 4. Molecular orbitals involved in the electronic transitions of W233 for differently substituted models.

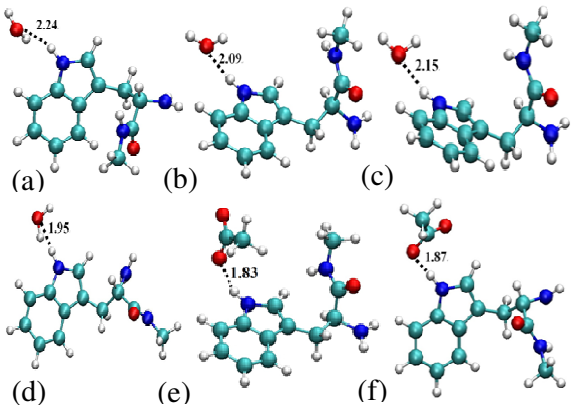

Fig. 5. Ball and stick models showing the intramolecular hydrogen bond distances (Å) between interfacial tryptophans and the neighboring water molecule or carboxyl group: (a) W198 with water, (b) W250 with water, (c) W302 with water, (d) W337 with water, (e) W94 with carboxyl group of D96 and (f) W233 with carboxyl group of D129.

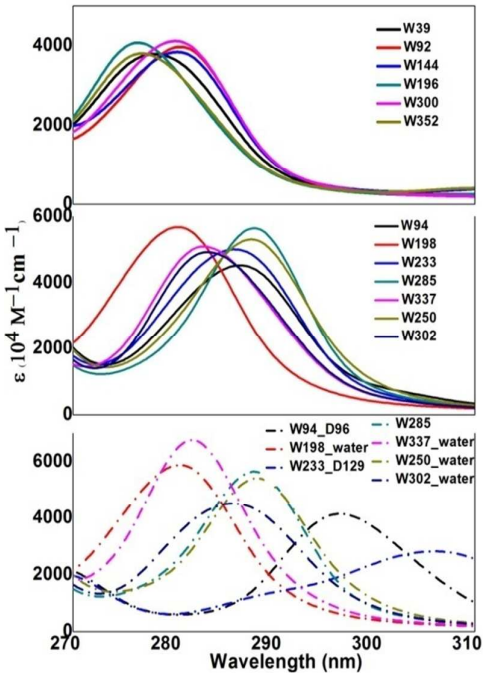

Fig. 6. Absorption spectra[22] of M7 for distal Trps (top panel), interfacial Trps (middle panel), and interfacial Trps with neighboring residues (bottom panel).

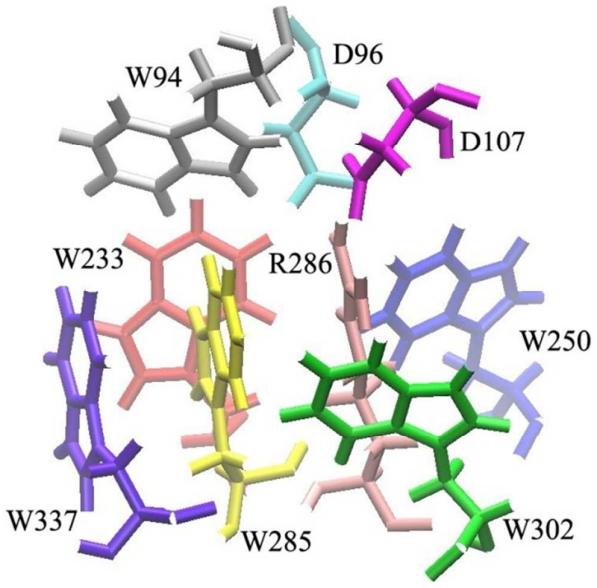

Fig.7. Configuration of clusters used for calculations of UV absorption spectra of UVR8.

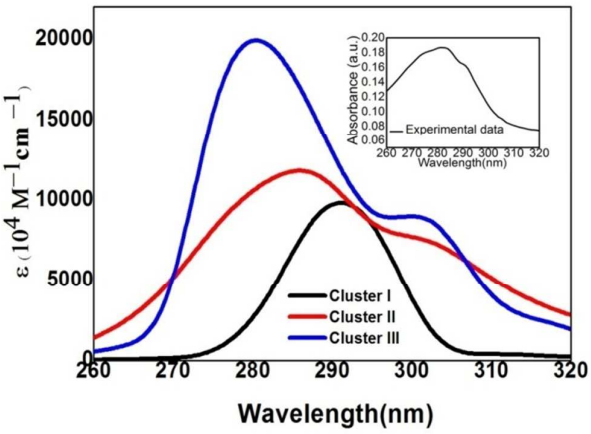

Fig. 8. Spectra[22] of the UVR8 amino acid cluster models.

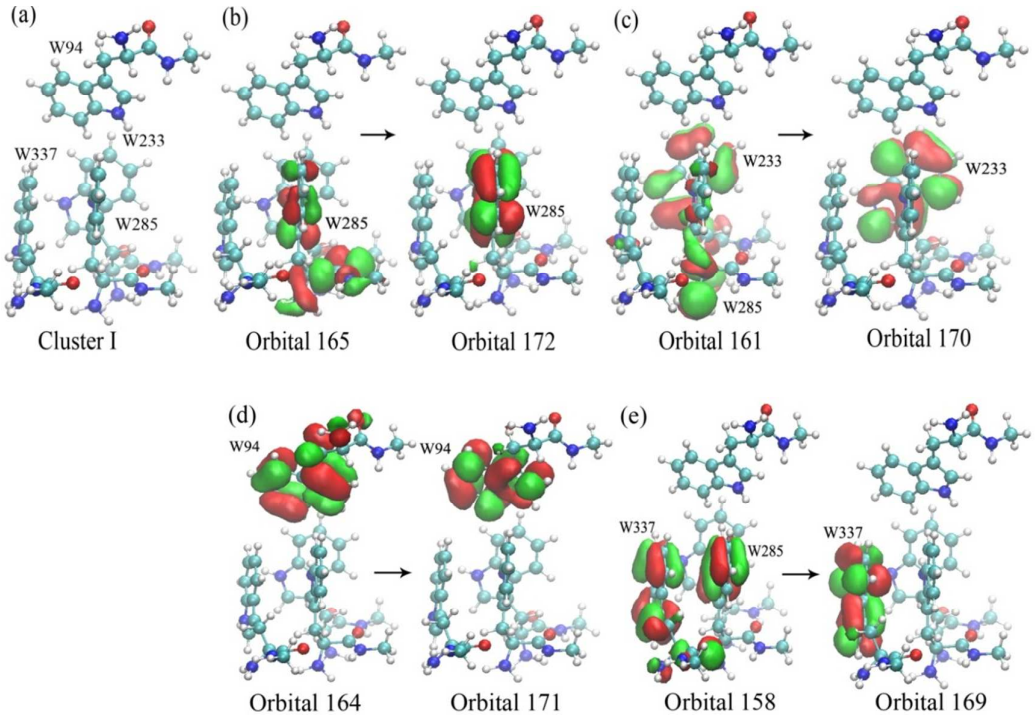

Fig. 9. Active orbitals involved in the transitions for (a) Cluster I at (b) 295.7 nm, (c) 286.9 nm, (d) 285.8 nm and (e) 283.9 nm. Occupied molecular orbitals are plotted on the left panel and unoccupied orbitals are plotted on the right in figures (b) to (e).

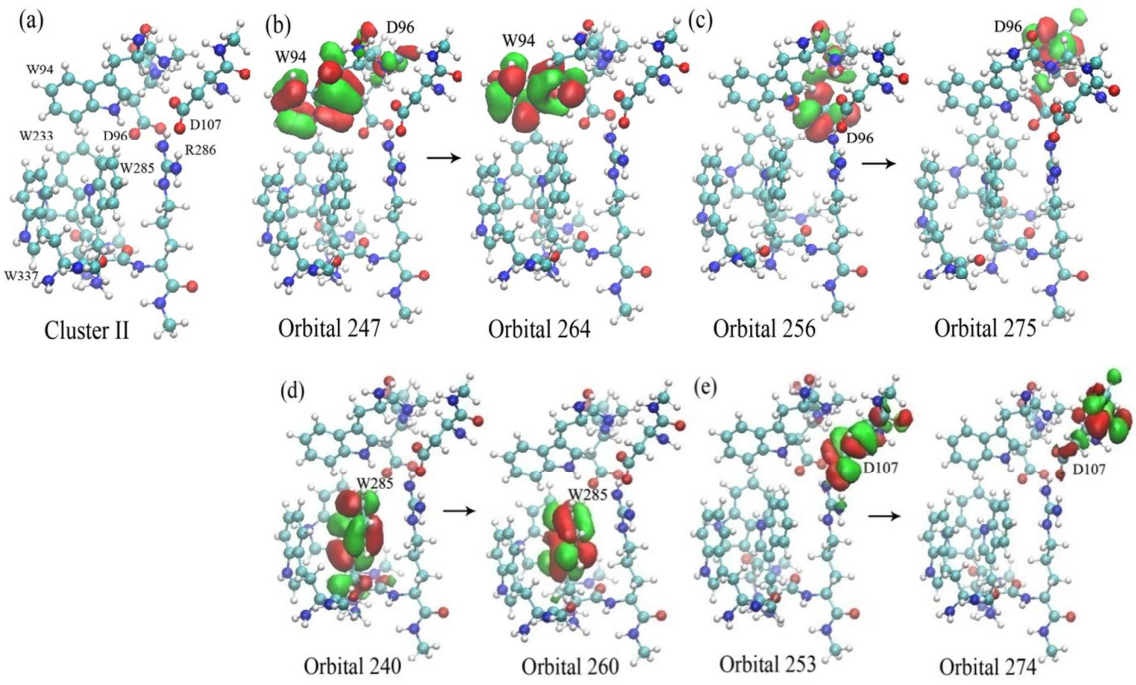

Fig. 10. Active orbitals involved in the transitions for (a) Cluster II at (b) 305.8 nm, (c)299.7 nm, (d) 290.1 nm and (e) 288 nm. Occupied molecular orbitals are plotted on the left panel and unoccupied orbitals are plotted on the right in figures (b) to (e).

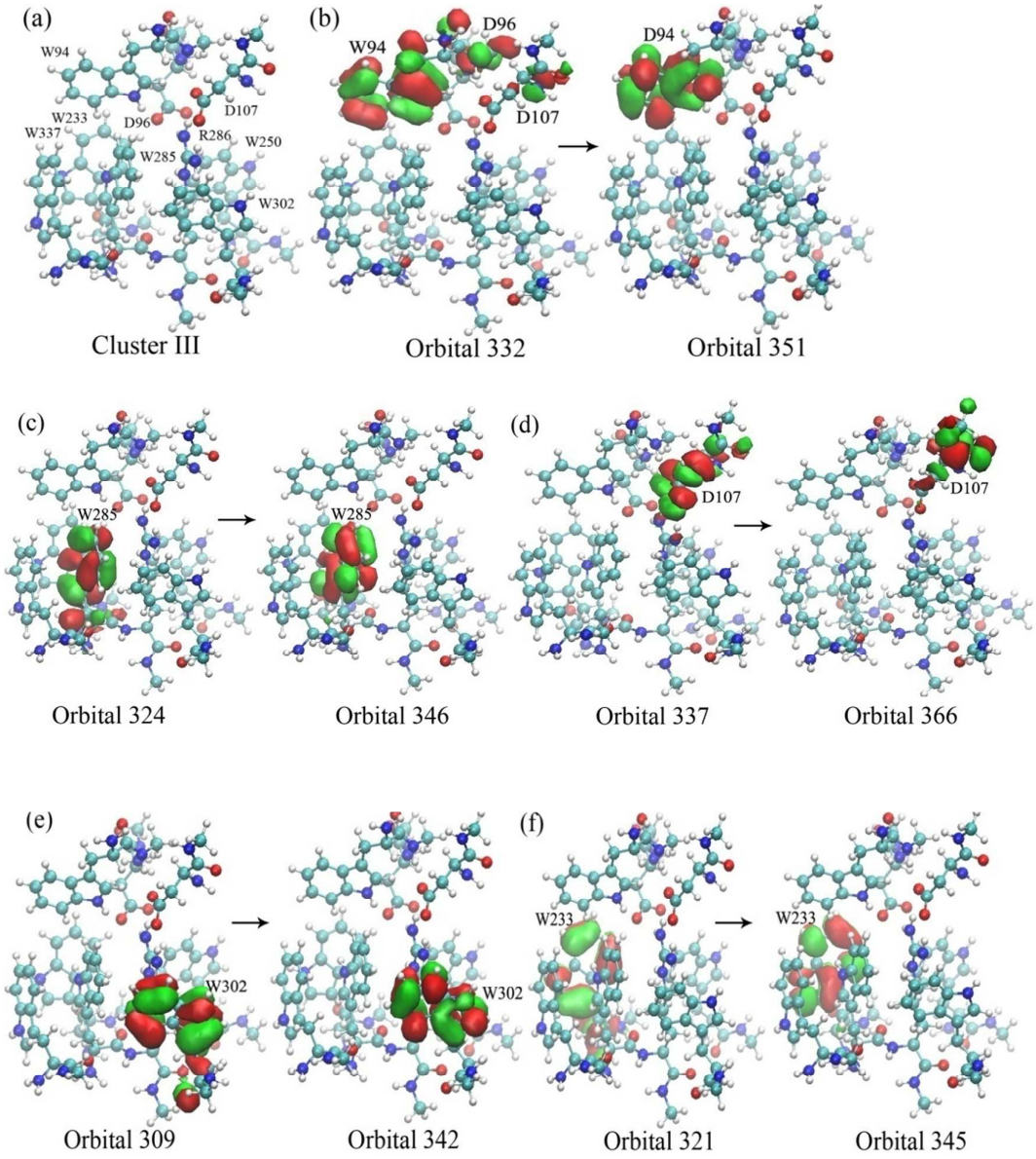

Fig. 11. Active orbitals involved in the transitions for (a) Cluster III at (b) 304.5 nm, (c) 291.4 nm, (d) 291.1 nm, (e) 285.6 nm and (f) 280.9 nm. Occupied molecular orbitals are plotted on the left panel and unoccupied orbitals are plotted on the right in figures (b) to (f).

REFERENCES

1 G. I. Jenkins, *Annu. Rev. Plant Biol.* 2009, **60,** 407-431.

2 N. R. Hofmann, *Plant Cell Online* 2012, **24,** 3485-3485.

3 M. Heijde and R. Ulm, *Trend Plant Sci.* 2012, **17,** 230-237.

4 L. Rizzini, J. J. Favory, C. Cloix, D. Faggionato, A. O'Hara, E. Kaiserli, R. Baumeister, E. Schafer, F. Nagy, G. I. Jenkins and R. Ulm, *Science* 2011, **332,** 103-106.

5 K. H. Gardner and F. Correa, *Science* 2012, **335,** 1451-1452.

6 J. M. Christie, A. S. Arvai, K. J. Baxter, M. Heilmann, A. J. Pratt, A. O'Hara, S. M. Kelly, M. Hothorn, B. O. Smith, K. Hitomi, G. I. Jenkins and E. D. Getzoff, *Science* 2012, **335,** 1492-1496.

7 W. Di, Q. Hu, Z. Yan, W. Chen, C. Yan, X. Huang, J. Zhang, P. Yang, H. Deng, J. Wang, X. Deng and Y. Shi, *Nature* 2012, **484,** 214-219.

8 A. O' Hara and G. I. Jenkins, *The Plant Cell* 2012, **24,** 3755-3766.

9 B. A. Brown, L. R. Headland and G. I. Jenkins, *Photochem.Photobiol.* 2009, **85,** 1147-1155.

10 C. Cloix, E. Kaiserli, M. Heilmann, K. J. Baxter, B. A. Brown, A. O'Hara, B. O. Smith, J. M. Christie and G. I. Jenkins, *ProcNatlAcadSci USA* 2012, **109,** 16366.

11 A. A. Voityuk, R. A. Marcus and M. E. Michel-Beyerle, *ProcNatlAcadSci USA* 2014, **111,** 5219-5224.

12 M. Wu, E. Grahn, L. A. Eriksson and Å. Strid, *J. Chem. Inf. Model.* 2011, **51,** 1287-1295.

13 D. Porezag, T. Frauenheim, T. Köhler, G. Seifert and R. Kaschner, *Phys. Rev. B* 1995, **51,** 12947-12957.

14 M. Elstner, D. Porezag, G. Jungnickel, J. Elsner, M. Haugk, T. Frauenheim, S. Suhai and G. Seifert, *Phys. Rev. B* 1998, **58,** 7260-7268.

15 T. Niehaus, S. Suhai, F. Della Sala, P. Lugli, M. Elstner, G. Seifert and T. Frauenheim, *Phys. Rev. B* 2001, **63,** 085108.

16 T. A. Niehaus, *J. Mol. Struct.: THEOCHEM* 2009, **914,** 38-49.

17 M. E. Casida, K. C. Casida and D. R. Salahub, *Int. J. Quant. Chem.* 1998, **70,** 933-941.

18 M. E. Casida and D. R. Salahub, *J. Chem. Phys.* 2000, **113,** 8918-8935.

19 M. J. Frisch, G. W. Trucks, H. B. Schlegel, G. E. Scuseria, M. A. Robb, J. R. Cheeseman, G. Scalmani, V. Barone, B. Mennucci, G. A. Petersson, H. Nakatsuji, M. Caricato, X. Li, H. P. Hratchian, A. F. Izmaylov, J. Bloino, G. Zheng, J. L. Sonnenberg, M. Hada, M. Ehara, K. Toyota, R. Fukuda, J. Hasegawa, M. Ishida, T. Nakajima, Y. Honda, O. Kitao, H. Nakai, T. Vreven, J. A. Montgomery, Jr., J. E. Peralta, F. Ogliaro, M. Bearpark, J. J. Heyd, E. Brothers, K. Kudin, N., V. N. Staroverov, R. Kobayashi, J. Normand, K. Raghavachari, A. Rendell, J. C. Burant, S. S. Iyengar, J. Tomasi, M. Cossi, N. Rega, N. J. Millam, M. Klene, J. E. Knox, J. B. Cross, V. Bakken, C. Adamo, J. Jaramillo, R. Gomperts, R. E. Stratmann, O. Yazyev, A. J. Austin, R. Cammi, C. Pomelli, J. W. Ochterski, R. L. Martin, K. Morokuma, V. G. Zakrzewski, G. A. Voth, P. Salvador, J. J. Dannenberg, S. Dapprich, A. D. Daniels, O. Farkas, J. B. Foresman, J. V. Ortiz, J. Cioslowski and D. J. Fox, Gaussian, Inc., Wallingford CT, Gaussian 09, Revision, A. 02, 2009.

20E. A. Perpète, V. Wathelet, J. Preat, C. Lambert and D. Jacquemin, *J. Chem. Theory Comput.* 2006, **2**, 434–440.

21D. Jacquemin, V. Wathelet,E. A. Perpète, C. Adamo, *J. Chem. Theory Comput.* 2009, **5**, 2420–2435.

22The y-axis represents the molar extinction coefficient, $\varepsilon = \sum_I \varepsilon_I$ .For its calculation we use the

relationship, $f_I = C\int \varepsilon_I(w)dw$,[29]where f_I is the oscillator strength related to excitation *I*, $C = 3.5\times10^{-5}\ \mathrm{M}\,cm/eV$ and the energy ω, is given in eV. By using Lorentzian functions for the spectral broadening, the extinction coefficient can then be written as, $\varepsilon(\omega) = \sum_I (f_I / C\pi)((\Gamma/2)/((\omega-\omega_I)+(\Gamma/2)^2))$. The parameter Γ specifying the function width was set to 0.1eV.

23 Y. A. Zolotarev, Y. A. Borisov, A. K. Dadayan and N. F. Myasoedov, *Amino Acids* 2006, **31,** 403-407.

24 X. Li, L. W. Chung, K. Morokuma and G. Li, *J. Chem. Theory Comput.* 2014, **10,** 3319-3330.

25 X. L. Zeng, Z. Ren, Q. Wu, J. Fan, P.-P. Peng, K. Tang, R. Q. Zhang, K.-H. Zhao and X. J. Yang, *Nature Plants* 2015, **1**, 14006.

26 L. Serrano-Andrés and B. O. Roos, *J. Am. Chem. Soc.* 1996, **118,** 185-195.

27 H. Lami, *J. Chem. Phys.* 1977, **67,** 3274.

28 A. Z. Britten and G. Lockwood, *Spectrochim. Acta* 1976, **32,** 1335-1338.

29N. J. Turro, V. Ramamurthy and J. C. Scaiano, in P*rinciples of Molecular Photochemistry: An Introduction*, ed. J. Stiefel, University Science Books: Sausalito, CA, 1st edn., 2009, pp 195–196.